CLASSIFICATION OF POLARIMETRIC-SAR DATA WITH NEURAL NETWORK USING COMBINED FEATURES EXTRACTED FROM SCATTERING MODELS AND TEXTURE ANALYSIS

KATMOKO ARI SAMBODO, ANIATI MURNI AND MAHDI KARTASASMITA

Abstract

This paper shows a study on an alternative method for classification of polarimelrioSAR data. The method is designed by integrating the combined features extracted from two scattering models (i.e.. Freeman decomposition model and Cloudc decomposition model) and lextural analysis with distribution-free neural network classifier. The neural network classifier (wich is based on a feed-forward back-propagation neural network architecture) properly exploits the information in the combined features for providing high accuracy classification results. The effectiveness of the proposed method is demonstrated using E-SAR polarimetric data acquired on the area of Penajam, East Kalimantan, Indonesia.

Keywords: Po/ahmeiric-SAR, scattering model. Freeman decomposition, Cloude decomposition, texture analysis, feature extraction, classification, neural networks.

I. Introduction

Fully polarimetric-SAR data can define the scattering behavior of land use/cover, thus giving better land use/cover classification results than single-channel single-polarization SAR data (Karathanassi and Dabboor, 2004; Woodhouse, 2006). Many different approaches for the so called target (polarimelric) decomposition have been proposed to extract the information about the scattering mechanisms of different nature, which can be employed to assist the interpretation and the classification of polarimetric-SAR data. Freeman decomposition model and Cloude decomposition model are the most intensively used decomposition method for this purpose, because they are based on more realistic scattering models, their simplicity and easy implementation for image processing (Lee *et al.*, 2006; Yamaguchi *et at.*, 2005). In Freeman decomposition model (Freeman and Durden, 1998), radar backscatter responses are decomposed into three basic scattering mechanisms: surface scattering, double bounce scattering, and volume scattering. Volume scattering is modeled by a cloud of randomly oriented dipoles for tree canopy and vegetation. Double-bounce scattering component is modeled by scattering from dihedrals, but allows for reflector surfaces with different dielectric properties, corresponding to, for example trunk-ground interaction in forest scatter. Surface or single-bounce scattering is modeled by a Bragg surface scatlerer. Cloude and Pottier (1997) proposed an unsupervised classification based on their target decomposition theory. The medium's scattering mechanism, characterized by entropy H and alpha angle a, are used for classification. The entropy H is a measure of randomness of scattering mechanisms, and the alpha angle a characterizes the scattering mechanisms. The H-a plane was divided into eight zones. The physical scattering characteristic associated with each zone provides information for terrain type assignment.

Lcmbaga Pcnerbangan dan Antariksa Nasional (LAPAN), JL Lapui No. 70, Pekavon, Pasar Rcbo, Jakarta. Indonesia.
Faculty of Computer Science, University oflndoncsiu. Kampus UI Depok. 16424. Indonesia,

These polarimetric decomposition methods have been found to be applicable to land cover classification (Cloudc and Potlicr, 1997; Freeman and Durdcn, 1998; Lumsdon 2003), sea ice classification (Scheuchl, 2001), and forest classification (Ferro-Famil *et al,* 2005; Lee *et al,* 2005). In general, they reported that applying decomposition polarimetric permits to identify in a macroscopic way the type of scattering mechanism. For example, open water and bare soils arc characterized by surface scattering. Scattering over forested areas is dominated by volume scattering while urban areas mainly characterized by double bounce scattering. However, in some cases they also observed that these schemes do not provide sufficient sensitivity especially for the separation of the volume scattering class and double scattering class. For example, urban areas (double scattering) are frequently interpreted as forest (volume scattering). It was also reported some limitation for further possibility to discriminate and classify into different object / land cover types in same scattering mechanism, for example, for classifying forested area into different forest types and growth stages.

In order to reduce inter-class ambiguity and improve the classification accuracy, further information has to be used. An analysis of the interferometric coherence can be useful to discriminate various types of forested area (Lee *et a/.,* 2005; Ferro-Famil *et al.,* 2005). However, this method works effectively if a pair of polarimetric interferometric data (i.e., two data of the same object acquired from different sensor positions) is available to compute the interferometric coherence information. In this paper, the consideration of additional information which can be extracted directly from a polarimetric image but using different aspect would be meaningful. A texture approach has been chosen which it can measure several aspects of spatial structure of an image. And we investigate how the textural features can be of help in discriminating different land-cover types. Textural features have a demonstrated ability to support image segmentation in many areas (Tso and Mather, 2001) and have also demonstrated potential for classifying sea ice types (Deng and Clausi, 2005; Clausi and Jemigan, 1998) and urban areas (Acqua and Gamba, 2003) in SAR imagery. Various texture methods are found in the research literature to extract textural features. For SAR image classification, it has been shown that the grey-level cooccurence matrix (GLCM) method is an effective method to generate appropriate textural features (Deng and Clausi, 2005; Tso and Mather, 2001).

The selection of the classification algorithm is critical issue in the classification of polarimetric data using multi-aspect information. When standard features associated with the intensity or amplitude of SAR signals arc exploited, maximum-likelihood classifiers are commonly used. However, our features are extracted from different aspect, so parametric classifiers become more difficult to use, as it is not possible to make reasonable assumptions on the class distributions of these combined features (Tso and Mather, 2001; Bruzzone *et at.,* 2004). In this paper, we propose a classification method that integrates the combined features extracted from two different aspects with distribution-free neural network classifier.

The proposed method is consisted of five main modules: 1) a pre-processing module; 2) a feature-extraction module based on scattering models; 3) a feature-extraction based on texture analysis; 4) a classification module based on neural network; and 5) a post-processing module.

The pre-processing module is based on a set of procedures commonly used in polarimetric-SAR data processing, we first prepare/construct scattering matrix from single look complex (SLC) data for each polarization, then apply speckle reduction filtering. The feature extraction module based on scattering models computes two sets of features derived from two polarimetric decomposition methods: Freeman decomposition and Cloude decomposition. The feature extraction module based on image texture computes a set of GLCM textural features. The classification module is based on feed-forward back-propagation neural network. The post-processing module is used to improve the classification result by correcting a possible misclassification of a pixel using the membership probability of pixel in its neighborhood. The block scheme of the proposed method is shown in Fig. 1.

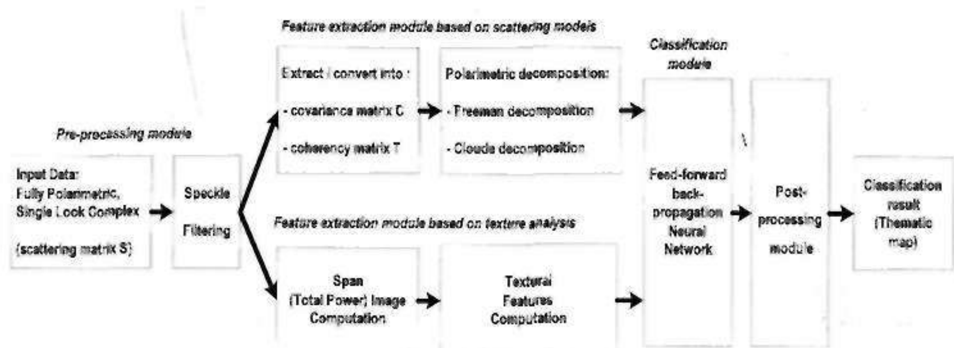

Fig. 1. Block scheme of the proposed method

The proposed method has been tested on a fully polarimetric E-SAR (L-Band) data acquired on the area of Penajam, East Kalimantan, Indonesia. We examined the method using: 1) the combined features of Freeman decomposition • model and textural features and 2) the combined features of Cloude decomposition and textural features, and compared both results.

This paper is organized into the following fashions. Section I is introductory. Section II briefly describes the feature extraction based on scattering models. Section III briefly presents feature extraction based on GLCM texture analysis. Section IV explains the classification module, which is based on feed-forward back-propagation neural network and post-processing techniques. The experimental results are reported in section V, and finally, Section VI provides a discussion and conclusion.

II. Feature Extraction based on Scattering Models

a. Polarimetric Data Representation

For radar polarimetry, the backscattering properties of the target can be completely described by a *2x2* complex scattering matrix, *S*, such that:

$$S = \begin{bmatrix} S_{hh} & S_{hv} \\ S_{vh} & S_{vv} \end{bmatrix} \quad (1)$$

where S_{hv} is the scattering element of horizontal transmitting and horizontal receiving polarization, and the other three elements are similarly defined. For the reciprocal backscattering case, $S_{hy} = S_{vh}$. The polarimetric scattering information can be represented by a target vector,

$$k = \left[S_{hh} \quad \sqrt{2}S_{hv} \quad S_{vv} \right]^{T} \qquad (2)$$

where the superscript "T" denotes the matrix transpose. The V2 on the $S_{/n}$, term is to ensure consistency in the span (total power) computation. Polarimetric information can also be represented by a covariance matrix C in the following form

$$C = kk^{*T} = \begin{bmatrix} |S_{hh}|^2 & \sqrt{2}S_{hh}S_{hv}^* & S_{hh}S_{vv}^* \\ \sqrt{2}S_{hv}S_{hh}^* & 2|S_{hv}|^2 & \sqrt{2}S_{hv}S_{vv}^* \\ S_{vv}S_{hh}^* & \sqrt{2}S_{vv}S_{hv}^* & |S_{vv}|^2 \end{bmatrix} \qquad (3)$$

where the superscript "*" denotes the complex conjugate. From (3), the span (or total power) is expressed as

$$SPAN = k^{*T}.k = |S_{hh}|^2 + 2|S_{hv}|^2 + |S_{vv}|^2 \qquad (4)$$

Alternatively, the Pauli based target vector k_p can be used to form coherency matrix T.

$$k_p = \frac{1}{\sqrt{2}}\left[S_{hh} + S_{vv} \quad S_{hh} - S_{vv} \quad 2S_{hv} \right]^{T} \qquad (5)$$

$$T = k_p . k_p^{*T} \qquad (6)$$

The coherency matrix representation has the advantage over the covariance matrix of relating to underlying physical scattering mechanisms (Lee *et ah,* 1999-a).

Fully polarimetric data provides unique possibility to separate scattering contributions of different nature, which can be associated to certain elementary scattering mechanisms. Several decomposition techniques have been proposed for this purpose. Freeman decomposition model and Cloude decomposition model are the most intensively used in several researches.

a.l. Feature Extraction based on Freeman Decomposition

The Freeman decomposition (Freeman and Durden, 1998) models is the covariance matrix C as the contribution of three basic scattering mechanisms: surface or single-bounce, double-bounce, and volume scattering. Volume scattering is modeled by a cloud of randomly oriented dipoles for tree canopy and vegetation. Double-bounce scattering is realistically described by scattering from dihedrals, but allows for reflector surfaces with different dielectric properties, corresponding to, for example trunk-ground interaction in forest scatter. Surface or single-bounce scattering is modeled by a Brag^g surface scatterer. Hence, the Freeman decomposition expresses the measured covariance matrix C as follows:

$$C = C_v + C_d + C_s \qquad (7)$$

where C_v, C_d, and C_s are covariance matrix corresponding to each scattering component (volume, double, surface) as presented in Table 1. From these matrices, then the contributions of each scattering mechanisms P_v, P_d, P_s to the span (total power) P can be estimated. These scattered powers P_v, RAb, P, can be employed to generate RGB image and can be used as classification features to allow differentiation between different land cover types (Freeman and Durden, 1998; Lumsdon, 2003).

$$P = P_v + P_d + P_s = \left(|S_{hh}|^2 + |S_{vv}|^2 + 2|S_{hv}|^2 \right) \qquad (8)$$

a.2. Feature Extraction based on Cloude Decomposition

The polarimetric decomposition theorem introduced by Cloude and Pottier (1997) proposed to identify polarimetric scattering mechanisms based on the eigenvalue analysis of a coherency matrix *T*. Applying eigenvalue analysis, the matrix *T* is decomposed into a sum of three coherence matrices *T*,, each weighted by its corresponding eigenvalue *X*,.

$$T=\sum_{i=1}^{3}\lambda_i T_i=\lambda_1(\mu_1.\mu_1^{*T})+\lambda_2(\mu_2.\mu_2^{*T})+\lambda_3(\mu_3.\mu_3^{*T}) \qquad (9)$$

Each matrix T_i is a unitary scattering matrix representing a deterministic scattering contribution. The amount of the contributions is given by the eigenvalues λ_i, while the type of scattering is related to the eigenvectors μ_i. The eigenvectors can be formulated as

$$\mu_i=\begin{bmatrix}\cos\alpha_i & \sin\alpha_i\cos\beta_i e^{i\delta} & \sin\alpha_i\sin\beta_i e^{i\gamma}\end{bmatrix}^T \qquad (10)$$

The α angle corresponds to the continuous change from surface scattering ($\alpha=0°$), moving into dipole or volume scattering ($\alpha=45°$), moving into double bounce scattering between two dielectric surfaces, and finally reaching dihedral scatter from metallic surfaces at $\alpha=90°$. The β angle is twice of the polarization orientation angle. The δ angle is the phase difference between the decomposed $S_{hh}+S_{vv}$ and $S_{hh}-S_{vv}$ terms, and the γ angle is the phase difference between the decomposed $S_{hh}+S_{vv}$ and S_{hv} terms. The ϕ angle is phase of the decomposed $S_{hh}+S_{vv}$ term.

Cloude and Pottier defined three secondary parameters, entropy H, anisotropy A, and mean alpha angle $\overline{\alpha}$, to characterize the result of the decomposition.

$$H=-\sum_{i=1}^{3}P_i\log_3 P_i \quad where\ P_i=\frac{\lambda_i}{\sum_{j=1}^{3}\lambda_j} \qquad (11)$$

$$A=\frac{\lambda_2-\lambda_3}{\lambda_2+\lambda_3} \qquad (12)$$

$$\overline{\alpha}=\sum_{i=1}^{3}P_i\alpha_i \qquad (13)$$

The entropy *H*, ranging from 0 to 1, represents the randomness of the scattering, with $H=0$ indicating a single scattering mechanism (isotropic scattering) and $H=1$ representing a random mixture of scattering mechanisms. For ocean and less rough surfaces, surface scattering will dominate, and ^/ is near 0. For heavily vegetated areas, the *H* value will be high, due to multiple scattering mechanisms. The anisotropy *A* represents the relative importance of the second and third scattering mechanisms. A high anisotropy states that only the second scattering mechanism is important, while a low anisotropy indicates that the third scattering mechanism also plays a role. The mean alpha angle *a* reveals the averaged scattering mechanisms from surface scattering *(a*—»0°), volume scattering («-»45°), to double bounce scattering («—> 90°). *H* and *a* clearly characterize the scattering characteristics of a medium.

Cloude and Pottier further suggest an unsupervised classification scheme, using the *H-a* plane sub-divide into 8 basic zones characteristic of different scattering behaviors, as shown in Fig. 2. However, this unsupervised estimation of the type of scattering mechanisms may reach some limitations due to the arbitrarily fixed linear boundaries in the *H-a* plane which may not fit to data distribution, leading to noisy classification results (Ferro-Famil *et at,* 2005; Lee *et at,* 1999-a). Hence, in this work, we use entropy *H,* anisotropy *A* , and mean alpha angle *a* directly as classification feature inputs to the neural network classifier.

Table 1. Three basic scattering mechanisms used in the Freeman decomposition model

Basic Scattering Mechanism	Model Scatterer	Corresponding Covariance Matrix	Scattered Power
Volume scattering	*Set of randomly oriented dipoles*  $S=\begin{bmatrix} S_h\cos^2\phi+S_v\sin^2\phi & (S_h-S_v)\cos\phi\sin\phi \\ (S_h-S_v)\cos\phi\sin\phi & S_h\sin^2\phi+S_v\cos^2\phi \end{bmatrix}$ Assumes thin cylindric scatterer ($S_v=1, S_h=0$)	$C_v=f_v\begin{bmatrix} 1 & 0 & 1/3 \\ 0 & 2/3 & 0 \\ 1/3 & 0 & 1 \end{bmatrix}$ $f_v=3\|S_{hv}\|^2$	$P_v=\frac{8f_v}{3}$
Double-bounce scattering	*Dihedral corner reflector*  $S=\begin{bmatrix} e^{j2\gamma_h}R_{gh}R_{th} & 0 \\ 0 & e^{j2\gamma_v}R_{gv}R_{tv} \end{bmatrix}$ R_g : Ground / Horizontal Surface Reflection Coefficient R_t : Trunk / Vertical Surface Reflection Coefficient γ : Attenuation & phase change effect	$C_d=f_d\begin{bmatrix} \|\alpha\|^2 & 0 & \alpha \\ 0 & 0 & 0 \\ \alpha^* & 0 & 1 \end{bmatrix}$ $\alpha=e^{j2(\gamma_h-\gamma_v)}\frac{R_{gh}R_{th}}{R_{gv}R_{tv}}$ $f_d=\|R_{gv}R_{tv}\|^2$	$P_d=f_d(1+\|\alpha\|^2)$
Surface or single-bounce scattering	*Bragg surface scatterer*  $S=\begin{bmatrix} R_h & 0 \\ 0 & R_v \end{bmatrix}$ R_h : Bragg Surface Reflection Coefficient for Horizontal Polarization R_v : Bragg Surface Reflection Coefficient for Vertical Polarization	$C_s=f_s\begin{bmatrix} \|\beta\|^2 & 0 & \beta \\ 0 & 0 & 0 \\ \beta^* & 0 & 1 \end{bmatrix}$ $\beta=\frac{R_h}{R_v}$ $f_s=\|R_v\|^2$	$P_s=f_s(1+\|\beta\|^2)$

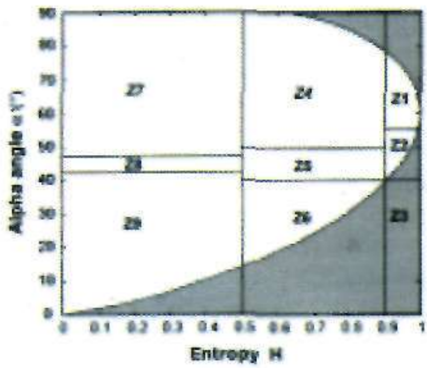

Physical scattering characteristics :
Z9 : Low Entropy Surface Scattering
Z8 : Low Entropy Dipole Scattering
Z7 : Low Entropy Multiple Scattering
Z6 : Medium Entropy Surface Scattering
Z5 : Medium Entropy Vegetation Scattering
Z4 : Medium Entropy Multiple Scattering
Z3 : (Not a Feasible Region in H- α space)
Z2 : High Entropy Vegetation Scattering
Z1 : High Entropy Multiple Scattering

Fig. 2. H - α plane

Then train the network sufficiently in a supervised method, and let the network to determine the optimal decision boundaries in feature space.

III. Feature Extraction based on Image Texture Analysis

Texture features calculated from grey-level cooccurrence matrices (GLCM) are often used for remote sensing image interpretation (Clausi and Jernigan, 1998; Acqua and Gamba, 2003; Tso and Mather, 2001), and the results have generally been successful. A GLCM contains the conditional-joint probabilities (P_t) of all pairwaise combinations of grey levels for a fixed window size *(N)* given two parameters: interpixel distance *(S)* and interpixel orientation *{$).* A different GLCM is required for each *(S, 0)* pair. Each GLCM is dimensioned to the number of quantized grey-levels *(G)*. Applying statistics to a GLCM generates different texture features. Eleven common features are presented in Table 2. These statistics extract several fundamental characteristics from the cooccurrence matrices. Moments about the main diagonal indicate the degree of smoothness of the texture (i.e., *contrast, dissimilarity,* and *inverse difference moment).* Another fundamental characteristic of the cooccurrence matrix is the uniformity of its entries (i.e., *entropy, maximum probability,* and *angular second moment).* If the grey-levels in the window tend to be homogeneous, then only a few grey-level pairs represent the texture. The features measure statistical property of GLCM (i.e., *mean, variance,* and *correlation).* And finally, features measure the grouping of pixels that have similar grey-level values (i.e., *cluster shade* and *cluster prominence).*

A shortcoming of determine texture features derived from GLCM is the excessive computational burden. For fully polarimetric images data, we can calculate textural features from four individual intensity images, i.e., HH, HV, VH, and VV images. However, this method may not be practical in terms of computational cost and make more complicated in interpretation due to large number of derived textural features. In this paper, we use only one span image, as calculated using (4). The span (or total power) image is a weighted average of HH, HV, and VV intensities and consequently has a lower speckle noise than HH, HV or VV individually. HH, HV, and W may have different scattering characteristics. Consequently, many features that may appear differently in each polarization, channel will show up in the span image (Lee era/., 1999-b).

Table 2. Some textural features extracted from GLCM

Textural Feature	Formula
Contrast	$\sum_{i,j=0}^{G-1} P_{i,j}(i-j)^2$
Dissimilarity	$\sum_{i,j=0}^{G-1} P_{i,j}\lvert i-j\rvert$
Inverse Difference Moment	$\sum_{i,j=0}^{G-1} \frac{P_{i,j}}{1+(i-j)^2}$
Angular Second Moment	$\sum_{i,j=0}^{G-1} P_{i,j}^{\ 2}$

Entropy	$-\sum_{i,j=0}^{G-1} P_{i,j} \log P_{i,j}$
Maximum Probability	$\max_{i,j}(P_{i,j})$
Mean	$\mu_i = \sum_{i,j=0}^{G-1} iP_{i,j}$, $\mu_j = \sum_{i,j=0}^{G-1} jP_{i,j}$
Variance	$\sigma_i^2 = \sum_{i,j=0}^{G-1} P_{i,j}(i-\mu_i)^2$, $\sigma_j^2 = \sum_{i,j=0}^{G-1} P_{i,j}(j-\mu_j)^2$
Correlation	$\sum_{i,j=0}^{G-1} P_{i,j}\left[\frac{(i-\mu_i)(j-\mu_j)}{\sigma_i\sigma_j}\right]$
Cluster Shade	$\sum_{i,j=0}^{G-1}((i-\mu_i)+(j-\mu_j))^3 P_{i,j}$
Cluster Prominence	$\sum_{i,j=0}^{G-1}((i-\mu_i)+(j-\mu_j))^4 P_{i,j}$

IV. Neural Network Classifier and Post-Processing Technique

a. Neural Network Classifier based on Feed-Forward Back-propagation Neural Network

The multilayer feed-forward using the back-propagation learning algorithm **is** one of the most widely used neural network. In this work, we apply multilayer feed-forward neural network architecture as depicted in Fig. 3., with an input layer, a hidden layer, and an output layer (Canty, 2006). The network contains L neurons in the hidden layer for classification of N-dimensional data into K classes.

The input layer accepts $N+1$ (biased) input feature vector g(v) ($g(v) = (1, g_1(v) \ldots g_N(v))^T$), and broadcast them to all of the L neurons in the hidden layer via weighted connections W. Neurons in the hidden layer sum all incoming signals and then computes its activation to form an ($L+1$)-component vector of intermediate outputs n(v) ($n(v) = (1, n_1(v) \ldots n_L(v))^T$). The logistic sigmoid function ($f(x) = 1/(1+e^{-x})$) is the most commonly used activation function. Intermediate outputs n(v) then transferred to all of the K neurons in the output layer via weighted connections W. Similarly, each neuron in the output layer sum of all incoming signals and then computes its activation to form the output signal m(v) ($m(v) = (m_1(v) \ldots m_K(v))^T$). However, in the output layer we use a modified logistic activation function for the output neurons, called softmax. The softmax function is defined as:

$$m_k(v) = \frac{e^{I_k^o(n(v))}}{e^{I_1^o(n(v))} + e^{I_2^o(n(v))} + \ldots + e^{I_K^o(n(v))}} \qquad (14)$$

where:

$$I_k^o(n(v)) = W_k^{oT} n(v), \quad k = 1 \ldots K \qquad (15)$$

This activation function, not only satisfy the condition $0 \le m_k(v) \le 1$, but also guarantee that the output signals sum to unity ($\sum_{k=1}^{K} m_k(v) = 1$). By using this activation function, the final network output will not only classify input feature vector into a class K (by selecting maximum value of m_k), but also generate class membership probability vectors **m(v)** for each observation. (These results will be used at post-processing module.)

Neural network must learn how to process inputs before they can be utilized in an application. According to the supervised learning scheme, the process of neural network training involves adjusting the weights on each layer (W ' and W) in such a manner that output of the network is consistent with the desired output (target class). The most well-known and extensively used for updating these weights is back-propagation learning algorithm. The back-propagation algorithm trains a neural network iteratively using a gradient descent algorithm in which the mean square error between the network output and the desired output is minimized. Once the network error has decreased to less than a specified threshold, the network has converged and is considered to be trained. However, the standard back-propagation learning algorithm is notoriously slow to convergence. To overcome this problem, we adopt two learning algorithms, i.e., Kalman filter and scaled conjugate gradient learning algorithm presented in Canty (2006). Learning process, then beginning with the former in order to approach a minimum (error) quickly, and then using the latter to refine the weights. Convergence is extremely fast when compared to standard back-propagation.

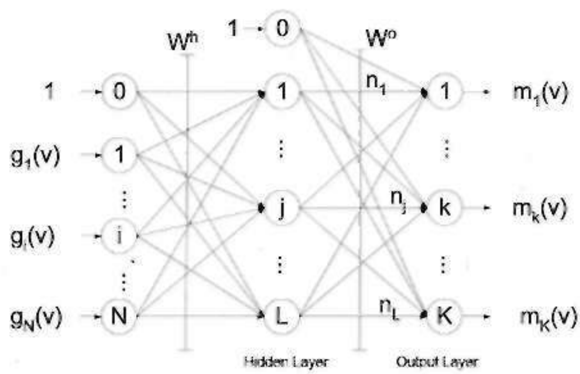

Fig. 3. A feed-forward neural network with L hidden neurons for classification of N-dimensional data into K classes.

b. Augmented-Vector Classification Method

The proposed method, as mentioned before, uses features extracted from two different aspects. In this work, we combine these features using *stacked-vector* or *augmented-vector* method as inputs to the classifier module, by simply extending the dimension of the data vectors to include each source from two aspects (Tso and Mather, 2001). For example, if we have three features extracted from scattering models and eleven features extracted from texture analysis, then fourteen features can be used together as inputs to the classifier module.

c. Post Processing Technique

Pixel-oriented classifiers sometimes provide classification result that contains misclassification at the pixel level that randomly distributed, and appear as "salt-and-pepper" effect in the classification map result. Richards and Jia proposed a method for correcting a possible misclassification of a pixel by examining the membership probability of the pixel in its neighborhood (Canty, 2006). They describe a method referred to as *probabilistic label relaxation,* which we have adapted here to improve our classification result and take spatial information into account. The class membership vectors m, $=(m_u...m_{Ki})^T$ are updated according to

$$\mathbf{m}_i' = \mathbf{m}_i * \frac{\mathbf{P}\,\mathbf{m}_n}{\mathbf{m}_i^T\,\mathbf{P}\,\mathbf{m}_n} \qquad (16)$$

where $P = (p)_w$ is a $K x K$ matrix of compatibility measures expressing the probability that a pixel in class k has a neighbor in class /, m„ is the average class membership vector for a 4-neighborhood of pixel i, and * denotes H adamard (component-by-component) multiplication. P is easily estimated directly from the originally classified image. The probabilistic label relaxation procedure can be iterated arbitrarily often. However too many iterations may lead to a widening of the effective neighborhood of a pixel to such an extent that irrelevant spatial information may falsify the final classification. Experiences show that the best results are obtained after *2-A* iterations.

V. Experimental Results

The proposed method is tested using single look complex (SLC) fully polarimetric-SAR data acquired over Penajam area, East Kalimantan Province. These data were acquired in L-band by Airborne E-SAR method on September 17th, 2004. The spatial resolution of the data used is 1.99 m and 3.0 m, in range and azimuth respectively. The scene under study contains different type of land covers: forest, fields, bare soils, and water area. Fig. 4 shows a set of ground survey information, and then by analyzing these data, a set of regions of interest (ROI) was defined. The whole ROI dataset then divide into two datasets, around 8.3% for training and around 91.7% for testing the neural network classifier (described in Table 3). From the testing dataset, we estimate the classification accuracy based on analysis of the confusion matrix.

As stated in Section IV, the feed-forward neural network classifier is consisted of three layers. The input layer has a number equal to a number of features of the used dataset, while output layer has a number equal to a number of classes to be recognized (i.e., four neurons in the classification of forest, fields, bare soils, and water area). However, then we must determine the number of neurons in the hidden layer. For this purpose, we carried experiments with classification using several combined features (3 features of scattering model and 11 textural features), and increase the number of hidden neurons incrementally (with 2, 10, 20, 30, 40, and 50). When a few neurons are used, the classification results are not satisfactory, whereas the larger number of the neurons cause longer neural network training times. We found that 30 neurons are the most appropriate selection in this experiment, larger then 30 neurons just provide slightly better classification performance. Then we used this neural network structure as classifier on the classification module.

For preprocessing, we construct scattering matrix from SLC data for each polarization and then apply speckle filtering using J.S. Lee Polarimetric Filter (Lee *et ah,* 1999-b). In order to investigate the effect of window size selection on classification performance, five windows: 3x3, 5x5, 7x7, 9x9 have been implemented, and without speckle filtering. In this experiment, larger then 9x9 windows is not used, because it causes too much blurring.

To extract GLCM textural features (11 features), first we compute the span images for filtered images using (4). In this experiment, these features are computed on a window size 15x15 pixels and grey-level quantization equal 64. The interpixel distance is set equal to one in all four interpixel orientations, i.e., 0, 45, 90, and 135° to account for possible directionality of the objects. Then classifications are performed for each data using neural network in order to determine the most appropriate textural feature sets. We observe that the highest accuracy, 84.30% is obtained from dataset without speckle filtering, and the classification result is shown in Fig. 7-b. (Filtering has the potential to reduce textural information from the image). Then we use these textural feature sets as combined features with other features extracted from scattering mQdels.

Table 3. Number of training and testing samples used in the experiments

Land-cover Class	Training Set	Testing Set
Water	761	8,361
Forest	348	3,822
Fields	284	3,128
Bare soils	302	3,327
Total Pixels	1,695	18,638

•	Water
•	Forest
	Fields
•	Bare soils

Fig. 4. Ground survey information

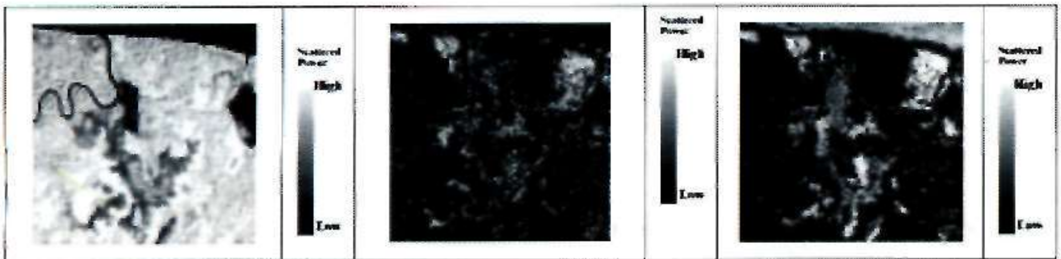

a) Volume scattering P_v | b) Double-bounce scattering P_d | c) Surface or single-bounce scattering P_s

Fig. 5. Features extracted from Freeman decomposition model

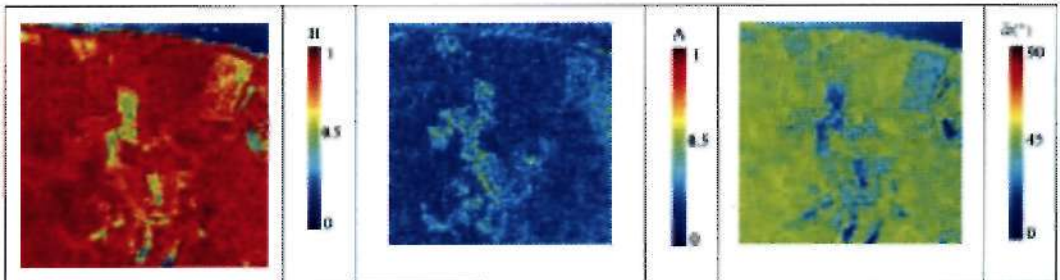

a) Entropy H | b) Anisotropy A | c) Mean Alpha Angle α

Fig. 6. Features extracted from Cloude decomposition model

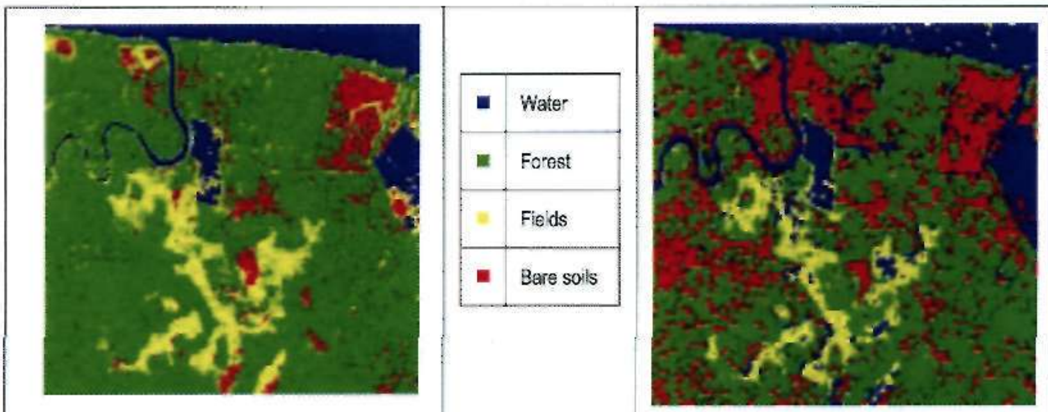

Reference Data / Classified Data	Water	Bare soils	Fields	Forest	User's Accuracy
Water	8354	0	43	0	99.49%
Bare soils	0	2946	52	331	88.49%
Fields	7	78	2815	155	92.14%
Forest	0	303	218	3336	86.49%
Producer's Accuracy	99.91%	88.54%	89.90%	87.28%	

Overall accuracy: 93.63%

a) Using neural network classifier with input: Freeman decomposition features (3 features)

Reference Data / Classified Data	Water	Bare soils	Fields	Forest	User's Accuracy
Water	8139	0	1514	1	84.30%
Bare soils	0	3020	0	329	90.17%
Fields	222	0	1261	200	74.92%
Forest	0	307	353	3292	83.30%
Producer's Accuracy	97.34%	90.77%	40.31%	86.13%	

Overall accuracy: 84.30%

b) Using neural network classifier with input: GLCM textural features (11 features)

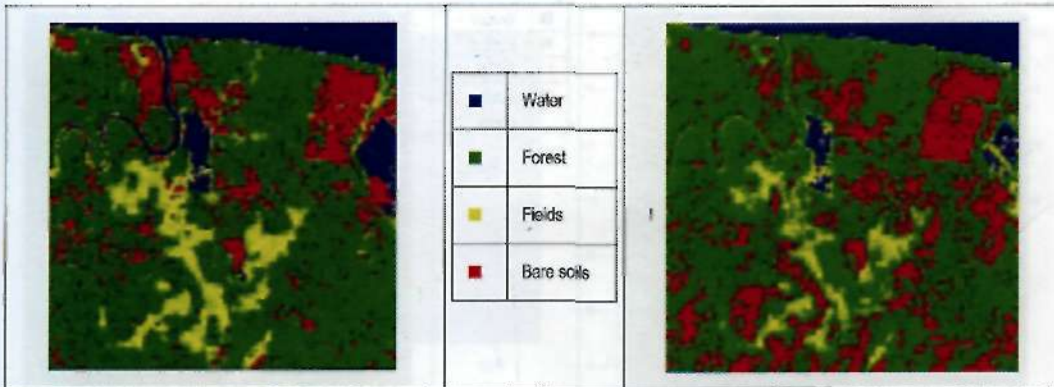

Reference Data / Classified Data	Water	Bare Soils	Fields	Forest	User's Accuracy
Water	8357	0	17	0	99.79%
Bare soils	0	3277	0	95	97.18%
Fields	4	1	3030	79	97.30%
Forest	0	49	81	3648	96.56%
Producer's Accuracy	99.95%	98.49%	96.86%	95.45%	

Overall accuracy: 98.25%

c) Using neural network classifier with input: Freeman decomposition + GLCM textural features (11 features)

Reference Data / Classified Data	Water	Bare soils	Fields	Forest	User's Accuracy
Water	8153	0	5	0	99.94%
Bare soils	0	3136	0	189	94.31%
Fields	206	0	2529	9	92.09%
Forest	0	191	594	3624	82.19%
Producer's Accuracy	97.51%	94.25%	80.85%	94.82%	

Overall accuracy: 93.58%

d) Using max. likelihood classifier with input: Freeman decomposition + GLCM textural features (11 features)

Figure. 7. Classification results (thematic map and confusion matrix of testing dataset) using neural network classifier with combined features of Freeman decomposition model and GLCM textural. These results are obtained with speckle filter window size equal to 7x7 pixels. (Classification result using maximum likelihood classifier is also presented as comparison)

To extract features based on scattering models, first we convert the scattering matrix representation into covariance matrix and coherency matrix using (3) and (6), respectively. Then, we apply Freeman decomposition and Cloude decomposition for each speckle-filtered data. Fig. 5 shows the features extraction results from Freeman decomposition. We can observe that this decomposition provide good discrimination of different land cover types. Forested areas is dominated by volume scattering while water areas mainly characterized by surface scattering. Surface scattering is still dominant for bare soils, but a significant amount of double bounce scattering is present. This indicates that a number of the fallen tree trunks and branches lying on the clear-cut areas may cause double-bounce scattering. However, the similar scattering mechanisms are also observed on field areas, and may cause poor separability between fields and bare soils. We then use these features as input for neural network classifier module. The classification result for 7x7 speckle-filtered data is shown in Fig. 7-a. High accuracy (93.63%) is obtained, but some misclassification between forest, fields, and bare soils occurred. However, when we combine these features with textural features, the classification accuracy is improved more than 4.5%. Results for each speckle-filtered data are shown in Fig. 9 (We plot the overall accuracy as a function of the window size of the speckle filter). It was found that for each case, the classification accuracy was improved by 3% ~ 20%.

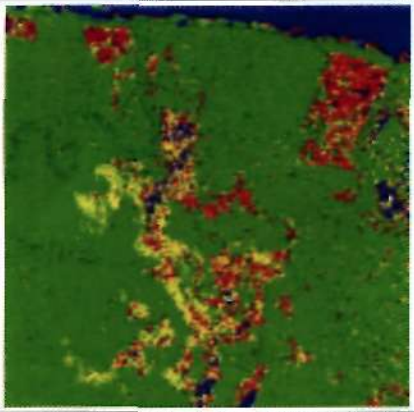

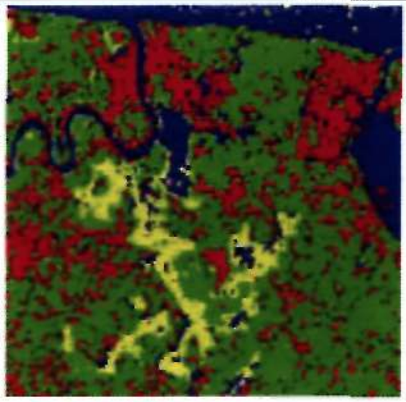

Reference Data / Classified Data	Water	Bare soils	Fields	Forest	User's Accuracy
Water	7728	131	62	24	97.29%
Bare soils	269	2306	590	158	69.30%
Fields	51	681	2000	175	68.80%
Forest	253	209	479	3485	78.70%
Producer's Accuracy	93.14%	69.31%	63.94%	90.58%	

Overall accuracy: 83.48%

a) Using neural network classifier with input: Cloude decomposition features (3 features)

Reference Data / Classified Data	Water	Bare soils	Fields	Forest	User's Accuracy
Water	8139	9	1514	1	84.30%
Bare soils	0	3028	0	329	90.17%
Fields	222	9	1281	208	74.92%
Forest	0	307	353	3292	83.30%
Producer's Accuracy	97.34%	90.77%	40.31%	86.13%	

Overall accuracy: 84.30%

b) Using neural network classifier with input: GLCM textural features (11 features)

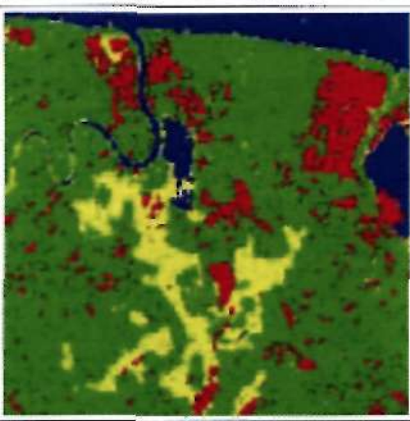

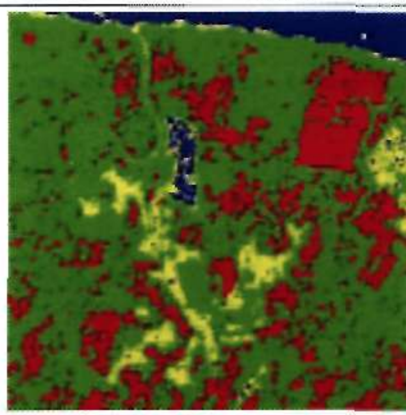

Reference Data / Classified Data	Water	Bare Soils	Fields	Forest	User's Accuracy
Water	8361	0	0	0	100%
Bare soils	0	3313	0	86	97.64%
Fields	0	0	3039	61	98.03%
Forest	0	14	89	3681	97.27%
Producer's Accuracy	100%	99.58%	97.15%	96.31%	

Overall accuracy: 98.69%

c) Using neural network classifier with input: Cloude decomposition + GLCM textural features (11 features)

Reference Data / Classified Data	Water	Bare soils	Fields	Forest	User's Accuracy
Water	7959	0	58	0	99.27%
Bare soils	9	2960	8	166	94.92%
Fields	457	0	2041	7	81.16%
Forest	35	377	1029	3667	71.73%
Producer's Accuracy	93.99%	88.67%	65.26%	95.56%	

Overall accuracy: 88.57%

d) Using max. likelihood classifier with input: Cloude decomposition + GLCM textural features (11 features)

Fig. 8. Classification results (thematic map and confusion matrix of testing dataset) using neural network classifier with combined features of Cloude decomposition model and GLCM textural. These results are obtained with speckle filter window size equal to 7x7 pixels. (Classification result using maximum likelihood classifier is also presented as comparison)

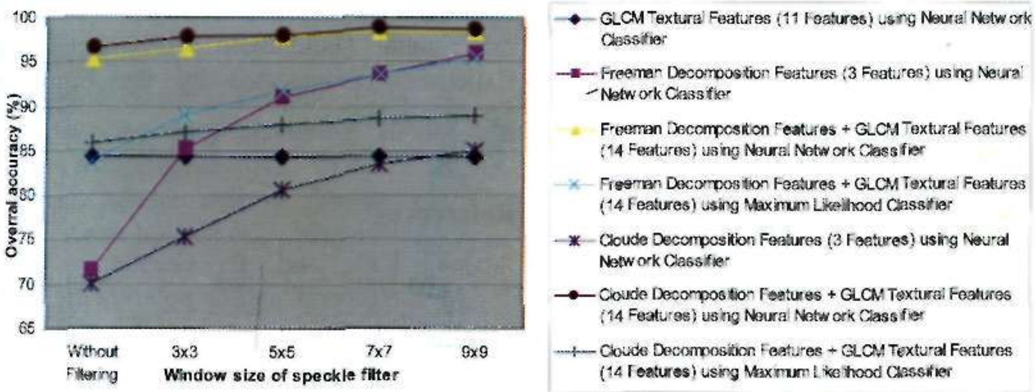

Fig. 9. Classification results for all the experiments. (Overall accuracy as a function of the window size of the speckle filter.)

Fig. 6 shows the features extraction results from Cloude decomposition. By analyzing mean alpha angle *a* and entropy *H*, we can observe that open water area is characterized by surface scattering (alpha values less than 42.5°) with low entropy, while forest area is characterized by volume scattering (alpha values near 45°) with high entropy ($H > 0.9$). Bare soils and fields are both characterized relatively by medium entropy and low alpha values, and may cause low separability between these two classes. Anisotropy *A* does not provide sufficient sensitivity for the separation of the different land-cover types, however, may be used for separation of the bare soil class and field class. We then use these features as input for neural network classifier module. The classification result for 7x7 speckle-filtered data is shown in Fig. 8-a. Overall accuracy 83.48% is obtained, with some misclassification between forest, fields, and bare soils are occurred evidently. It can also be observed that water class at river areas can not be accurately identified. However, when we combine these features with textural features, the classification accuracy is significantly improved more than 15%. Results for each speckle-filtered data are shown in Fig. 9. It was found that for each case, the classification accuracy was improved by 13% ~ 25%.

In order to point out the improvements that can be obtained with the classification module defined in our method, we compared the results of the neural network classifier with those obtained when classifying the combined features dataset with maximum likelihood classifier. In all trials, we observed that the accuracies exhibited by the neural network are always higher (3%~11%) than by maximum likelihood classifier (shown in Fig. 9). These results can also be confirmed in Fig. 7-d and Fig. 8-d, which some misclassification between forest, fields, and bare soils are occurred evidently, and water class at river areas can not be accurately identified by maximum likelihood classifier.

VI. Conclusion

A method for supervised classification of polarimetric-SAR data has been proposed. The method was designed by integrating the combined features extracted from two scattering models (i.e., Freeman decomposition model and Cloude decomposition model) and textural analysis (based on GLCM) with distribution-free neural network classifier.

The proposed method has been tested on a fully polarimetric, single look complex E-SAR (L-Band) data acquired on the area of Penajam, East Kalimantan, Indonesia. From an analysis of the results of all the experiments carried out using this method, we can conclude that the scattering model features alone can discriminate different land-cover types with reasonable accuracy while adding textural features can help to further improve the classification performance. In detail investigation, we verified that: 1) the accuracy improvement for combined features of cloude decomposition model and textural analysis is higher than for combined features of Freeman decomposition model and textural analysis; and 2) distribution-free neural network classifiers are very effective classification methodology that allows to exploit the information in the two above combined features (3%~11% better than maximum likelihood classifiers).

In future work, we intend to extend the scope of the method to include another aspect, such as polarimetric discriminators (Woodhouse, 2006) or features extracted from other frequency-SAR, and test the method on more complex area or land-cover types.

Acknowledgement

The authors would like to thank The Ministry of Forestry Republic of Indonesia for providing the E-SAR polarimetric data. The used polarimetric data set was acquired through INDREX-II experiment (Indonesian Airborne Radar Experiment) supported by the European Space Agency.

References

Acqua, F.D. and P. Gamba. 2003. Multitemporal and/or polarimetric SAR characterization of urban areas, in *Proceedings of the Workshop on POLINSAR - Applications of SAR Polarimetry and Polarimetric Interferometry.*

Bruzzone, L., M. Marconcini, U. Wegmuller, and A. Wiesmann. 2004. An Advanced method for the automatic classification of multitemporal SAR images, *IEEE Trans. Geosci. Remote Sensing*, vol. 42, no. 6, pp. 1321-1334, Jun. 2004.

Canty, M.J. 2006. *Image Analysis, Classification and Change Detection in Remote Sensing*, CRC Press.

Clausi, D.A. and M.E. Jernigan. 1998. A fast method to determine co-occurrence texture features, *IEEE Trans. Geosci. Remote Sensing*, vol. 36, no. 1, pp. 298-300, Jan. 1998.

Cloude, S.R. and E. Pottier. 1997. An entropy based classification scheme for land applications of polarimetric SAR, *IEEE Trans. Geosci. Remote Sensing*, vol. 35, no. 1, pp. 68-78, Jan 1997.

Deng, H. and D. Clausi. 2005. Unsupervised segmentation of SAR sea ice imagery, *IEEE Trans. Geosci. Remote Sensing*, vol. 43, no. 3, pp. 528-538, Mar. 2005.

Ferro-Famil, L., E. Pottier, H. Skriver, P. Lumsdon, R. Moshammer, and K. Papathanassiou. 2005. Forest mapping and classification using L-Band Polinsar data, in *Proceedings of the Workshop on POLINSAR - Applications of SAR*

Polahmetry and Polarimetric Interferometry.

Freeman, A. and S.L. Durden. 1998. A three-componeni scattering model for polarimetric SAR data, *IEEE Trans. Geosci. Remote Sensing,* vol. 36, no. 3, pp. 963-973, May 1998.

Karathanassi, V. and M. Dabboor. 2004. Land cover classification using E-SAR polarimetric data, in *Proceedings of the XXth ISPRS Congress.*

Lee, J.S., M.R. Gnines, TX. Ainsworth, L.J. Du, D.L. Schuler, and S.R. Cloude. 1999. Unsupervised classification using polarimetric decomposition and the complex Wishart classifier, *IEEE Trans. Geosci. Remote Sensing,* vol. 37, no. 5, pp. 2249-2258, Sep. 1999-a.

Lee, J.S., M.R. Grunes, and G. D. Grandi. 1999. Polarimetric SAR speckle filtering and its impact on terrain classification, *IEEE Trans. Geosci. Remote Sensing,* vol. 37, no. 5, pp. 2363-2373, Sep. 1999-b.

Lee, J.S., M.R. Grunes, TX. Ainsworth, l.Hajnsek, T. Mette, and K.P. Papathanassiou. 2005. Forest classification bascd-on L-band polarimetric and interferometric SAR data, in *Proceedings of the Workshop on POLINSAR - Applications of SAR Polarimetry and Polarimetric Interferometry.*

Lee, J.S., M.R. Grunes, D.L. Schuler, E. Pottier, and L. Fenro-Famil. 2005. Scattering-model-based speckle filtering of polarimetric SAR data, *IEEE Trans. Geosci. Remote Sensing,* vol. 44, no. 1, pp. 176-187, Jan. 2006.

Lumsdon, P. 2003. Land cover classification and height estimation in polarimetric SAR interferometry", in *Proceedings of the Workshop on POLINSAR - Applications of SAR Polarimetry and Polarimetric Interferometry.*

Scheuchl, B., R. Caves, I. Cumming, and G. Staples. 2001. H/A/*a* -based classification of sea ice using SAR polarimetry, in *Proceedings of the 23rd Canadian Symposium on Remote Sensing.*

Tso, B. and P.M. Mather. 2001. *Classification Methods for Remotely Sensed Data,* Taylor & Francis Inc.

Woodhouse, I. 2006. *Introduction to Microwave Remote Sensing,* CRC Press.

Yamaguchi, Y., T. Moriyama, M. Ishido, and H. Yamada. 2005. Four-Component scattering model for polarimetric SAR image decomposition". *IEEE Trans. Geosci. Remote Sensing,* vol. 43, no. 8, pp. 1699-1706, Aug. 2005.